Earth's Future

RESEARCH ARTICLE
10.1029/2020EF001665

TROPOMI NO_2 in the United States: A Detailed Look at the Annual Averages, Weekly Cycles, Effects of Temperature, and Correlation With Surface NO_2 Concentrations

Daniel L. Goldberg[1,2], Susan C. Anenberg[1], Gaige Hunter Kerr[1], Arash Mohegh[1], Zifeng Lu[2], and David G. Streets[2]

[1]Department of Environmental and Occupational Health, George Washington University, Washington, DC, USA, [2]Energy Systems Division, Argonne National Laboratory, Argonne, IL, USA

Key Points:

- The high instrument sensitivity of Tropospheric Monitoring Instrument (TROPOMI) can measure NO_2 pollution with unprecedented clarity compared to predecessor instruments
- We can now quantify pollution hotspots within cities such as those related to airport/shipping operations and high traffic areas
- Annual column NO_2 observed by TROPOMI has good correlation ($R^2 = 0.66$) with EPA surface observations without any surface-to-column conversion

Supporting Information:

- Supporting Information S1

Correspondence to:
D. L. Goldberg,
dgoldberg@gwu.edu

Citation:
Goldberg, D. L., Anenberg, S. C., Kerr, G. H., Mohegh, A., Lu, Z., & Streets, D. G. (2021). TROPOMI NO_2 in the United States: A detailed look at the annual averages, weekly cycles, effects of temperature, and correlation with surface NO_2 concentrations. *Earth's Future*, *9*, e2020EF001665. https://doi.org/10.1029/2020EF001665

Received 17 JUN 2020
Accepted 10 FEB 2021

Author Contributions:
Conceptualization: Daniel L. Goldberg
Data curation: Daniel L. Goldberg, Arash Mohegh, Zifeng Lu
Formal analysis: Daniel L. Goldberg, Gaige Hunter Kerr

© 2021. UChicago Argonne, LLC, Operator National Laboratory.
Earth's Future published by Wiley Periodicals LLC on behalf of American Geophysical Union.
This is an open access article under the terms of the Creative Commons Attribution License, which permits use, distribution and reproduction in any medium, provided the original work is properly cited.

Abstract Observing the spatial heterogeneities of NO_2 air pollution is an important first step in quantifying NO_X emissions and exposures. This study investigates the capabilities of the Tropospheric Monitoring Instrument (TROPOMI) in observing the spatial and temporal patterns of NO_2 pollution in the continental United States. The unprecedented sensitivity of the sensor can differentiate the fine-scale spatial heterogeneities in urban areas, such as emissions related to airport/shipping operations and high traffic, and the relatively small emission sources in rural areas, such as power plants and mining operations. We then examine NO_2 columns by day-of-the-week and find that Saturday and Sunday concentrations are 16% and 24% lower respectively, than during weekdays. We also analyze the correlation of daily maximum 2-m temperatures and NO_2 column amounts and find that NO_2 is larger on the hottest days (>32°C) as compared to warm days (26°C–32°C), which is in contrast to a general decrease in NO_2 with increasing temperature at moderate temperatures. Finally, we demonstrate that a linear regression fit of 2019 annual TROPOMI NO_2 data to annual surface-level concentrations yields relatively strong correlation ($R^2 = 0.66$). These new developments make TROPOMI NO_2 satellite data advantageous for policymakers and public health officials, who request information at high spatial resolution and short timescales, in order to assess, devise, and evaluate regulations.

Plain Language Summary Nitrogen oxides are a group of air pollutants released after fossil fuel combustion. A constituent of nitrogen oxides, nitrogen dioxide (NO_2), can be observed by satellite instruments due to its chemical properties. In this project, we average together images of NO_2 pollution gathered by the Tropospheric Monitoring Instrument satellite instrument over the United States in order to better determine the spatial distribution of NO2 air pollution. We find that this newest satellite instrument can observe air pollution with unprecedented clarity, similar to how HDTV is an advancement over regular TV. For example, we quantify pollution near individual airports, shipping areas, and major interstates; previous satellite instruments were unable to quantify air pollution with this type of precision. We also average the satellite data over different intervals to better determine cycles of air pollution. We find that NO_2 air pollution is 16% lower on Saturdays and 24% lower on Sundays. Additionally, we find that NO_2 pollution is larger on the hottest summer days as compared to typical summer days. These developments demonstrate how this new satellite instrument can advantageous for policymakers and health officials, who request information at high spatial resolution and short timescales, in order to assess, devise, and evaluate regulations

1. Introduction

Enhancements of NO_2 serve as a stark reminder of our society's global reliance on fossil-fuel combustion. NO_2—which comprises ~70% of NO_X ($NO_X = NO + NO_2$) in urban airsheds (Valin et al., 2013)—primarily originates as a byproduct of fossil-fuel combustion, although there are some biogenic sources of NO_2 such as lightning and microbes in soil (Jacob, 2000). NO_2 is a toxic air pollutant, which can cause and exacerbate asthma in vulnerable populations (Achakulwisut et al., 2019; Anenberg et al., 2018) and lead to premature mortality (Burnett et al., 2004). NO_2 can also react in the atmosphere to create tropospheric ozone (O_3), which is noted for its damaging effects including premature aging of lungs (Broeckaert et al., 1999;

Funding acquisition: Daniel L. Goldberg, Susan C. Anenberg, David G. Streets
Investigation: Daniel L. Goldberg, Gaige Hunter Kerr
Methodology: Daniel L. Goldberg
Project Administration: Daniel L. Goldberg, Susan C. Anenberg, David G. Streets
Resources: Daniel L. Goldberg
Software: Daniel L. Goldberg, Arash Mohegh, Zifeng Lu
Validation: Daniel L. Goldberg
Writing – original draft: Daniel L. Goldberg
Writing – review & editing: Daniel L. Goldberg, Susan C. Anenberg, Gaige Hunter Kerr, Arash Mohegh, Zifeng Lu, David G. Streets

McConnell et al., 2002) and premature mortality (Bell, 2004; Bell et al., 2006). HNO_3 often represents the final chemical state of NO_2 in the atmosphere and when deposited, agitates the equilibrium of our ecosystems due to its acidic properties (Burns et al., 2016). NO_2 can also participate in a series of reactions to create particulate nitrate (NO_3^-), a component of fine particulate matter less than 2.5 microns in diameter ($PM_{2.5}$), which is the leading cause of mortality due to air pollution (Cohen et al., 2017).

There is a rich legacy of monitoring NO_2 by remote sensing instruments (Burrows et al., 1999). NO_2 can be observed from space because it has unique high-frequency spectral features within the 400–500 nm wavelength region (Vandaele et al., 1998). The newest remote sensing spectrometer, Tropospheric Monitoring Instrument (TROPOMI) (VanGeffen et al., 2019; Veefkind et al., 2012), has been gathering data on the global heterogeneities of NO_2 air pollution since October 2017. This instrument builds on the legacy of prior Ultraviolet – Visible (UV-Vis) spectrometers including the Global Ozone Monitoring Experiment (GOME) (Burrows et al., 1999; Martin et al., 2002; Richter & Burrows, 2002), the Scanning Imaging Spectrometer for Atmospheric Chartography (SCIAMACHY) (Bovensmann et al., 1999; Heue et al., 2005), the Global Ozone Monitoring Experiment - 2 (GOME-2) instrument (Munro et al., 2016; Richter et al., 2011), and the Ozone Monitoring Instrument (OMI) (Boersma, Eskes, Richter, et al., 2018; Krotkov, Lamsal, et al., 2017; Levelt, Oord, et al., 2006, Levelt, Joiner, et al., 2018).

Satellite-based remote sensing instruments can be particularly useful in quantifying the trends of NO_X pollution in high-emission areas (Castellanos & Boersma, 2012; Duncan et al., 2016; Georgoulias et al., 2019; Krotkov, McLinden, et al., 2016; McLinden et al., 2016; Stavrakou, Müller, Boersma, et al., 2008; Van Der A et al., 2008), the seasonal cycles of air pollution (Ialongo, Herman et al, 2016; Shah et al., 2020), and the weekly cycle of NO_X emissions (Beirle, Platt, et al., 2003; de Foy, Lu, & Streets, 2016; Ialongo, Herman et al, 2016; Ma et al., 2013; Russell, Valin, et al., 2010; Stavrakou, Müller, Bauwens, et al., 2020; Valin et al., 2014). In an additional step, NO_X emissions can be computed by combining the satellite data with meteorological information (Beirle, Borger, et al., 2019, Beirle, Boersma, et al., 2011; de Foy, Lu, Streets, Lamsal, & Duncan, 2015; Goldberg, Lu, Streets, et al., 2019; Goldberg, Saide, et al., 2019; Lorente, Boersma, et al., 2019; Lu et al., 2015; Valin et al., 2013) or by combining the satellite data with chemical transport models (Canty et al., 2015; Cooper, Martin, Padmanabhan, & Henze, 2017; Elissavet Koukouli et al., 2018; Mijling & Van Der A, 2012; Qu et al., 2017; Souri et al., 2016). Due to the consistency and robustness of the remotely sensed NO_2 data record, scientists are beginning to infer information from the NO_2 data about other trace gases such as CO_2 (Goldberg, Lu, Oda, et al., 2019; Konovalov et al., 2016; Reuter et al., 2019), CH_4 (de Gouw et al., 2020), and CO (Lama et al., 2020), since remotely sensed measurements of those trace gases are generally less reliable. Therefore, remotely sensed NO_2 can also be helpful in indirectly estimating greenhouse gas emissions.

TROPOMI's smallest pixel size (3.5×7.2 km^2 at nadir, reduced to 3.5×5.6 km^2 at nadir on 6 August 2019) and enhanced sensitivity are significant improvements when compared to previous satellite instruments (Veefkind et al., 2012). NO_2 is unique due to its relatively short photochemical lifetime which varies from 2 to 5 h during the summer daytime (Beirle, Boersma, et al., 2011; de Foy, B., Wilkins, J. L., et al., 2014; Laughner & Cohen, 2019; Valin et al., 2013) to 12–24 h during winter (Shah et al., 2020). As a result, tropospheric NO_2 concentrations are strongly correlated with local NO_X emissions, which are often anthropogenic in origin.

Initial NO_2 measurements from TROPOMI show the complex spatial heterogeneities of NO_2 pollution with more refined resolution than any instrument before it (Griffin et al., 2019; Ialongo, Virta, et al., 2020). In particular, the smaller pixel sizes aid researchers in differentiating pollution sources within a single metropolitan area such as isolating signals from airports and individual highways (Judd, Al-Saadi, Janz, et al., 2019). These small-scale pixel sizes also show better agreement with the spatial features suggested by ground-based measurements (Ialongo, Virta, et al., 2020; Judd, Al-Saadi, Janz, et al., 2019). In particular, modeling studies have shown that matching the city-wide NO_2 column to 10% accuracy requires a spatial resolution of at least 4 km (Valin, Russell, Hudman, & Cohen, 2011)—the approximate spatial resolution of TROPOMI. Robust high-spatial resolution estimates are also critical inputs to those trying to quantify the surface-level NO_2 exposures (Geddes, Martin, et al., 2016; Lamsal et al., 2008; Larkin et al., 2017).

The improved spatial resolution and instrument sensitivity also allow for shorter temporal averaging ranges (days to months) to gain the similar spatial structure it would normally take >1 year to gather (Beirle, Borger, et al., 2019; Dix et al., 2020; Goldberg, Lu, Streets, et al., 2019; Lorente, Boersma, et al., 2019). As a result, it is easier to gain insight on the short-term variations of NO_X pollution when using TROPOMI, which can be especially helpful for those trying to quantify intra-annual changes in NO_X emissions (F. Liu et al., 2020).

In this paper, we exploit TROPOMI's small pixel sizes and enhanced instrument sensitivity to analyze spatial and temporal features of NO_X columns in the continental United States on annual, seasonal, weekly, and daily timescales. For example, using only a short temporal range of data, we can now answer such questions as:

- Which location within each U.S. state has the worst NO_2 air pollution?
- How does the NO_X emissions cycle vary by day of the week?
- How does temperature affect column NO_2 amounts?
- How well can we infer surface-level concentrations from satellite data?

While older sensors (e.g., OMI) provided insight into some of these questions, early sensors lacked the same sensitivity and required longer oversampling times. Therefore, answers illuminated by TROPOMI provide a "clarity" that has not been seen before.

2. Methods

2.1. TROPOMI NO_2

TROPOMI was launched by the European Space Agency for the European Union's Copernicus Sentinel 5 Precursor (S5p) satellite mission on 13 October 2017. The satellite follows a sun-synchronous, low-earth (825 km) orbit with an equator overpass time of approximately 13:30 local solar time (Veefkind et al., 2012). TROPOMI measures total column amounts of several trace gases in the Ultraviolet-Visible-Near Infrared-Shortwave Infrared spectral regions (VanGeffen et al., 2019). This instrument is characterized as a passive optical satellite sensor due to its reliance on solar UV-Visible radiation to gather measurements. At nadir, pixel sizes are 3.5×7 km^2 (reduced to 3.5×5.6 km^2 on 6 August 2019) with little variation in pixel sizes across the 2,600 km swath. The instrument observes the swath approximately once every second and orbits the Earth in about 100 min, resulting in daily global coverage.

Using a differential optical absorption spectroscopy technique on the radiance measurements in the 405–465 nm spectral window, the top-of-atmosphere spectral radiances can be converted into slant column amounts of NO_2 between the sensor and the Earth's surface (van Geffen et al., 2020). In two additional steps, the slant column quantity can be converted into a tropospheric vertical column content. In the first step, the stratospheric portion of the column (the amount above approximately 12 km in altitude) is subtracted using a global model estimate that is refined using data assimilation (Boersma, Eskes, & Brinksma, 2004). In a second step, the slant tropospheric column is converted to a vertical column using a quantity known as the air mass factor (AMF). The AMF is the most uncertain quantity in the retrieval algorithm (Lorente, Folkert Boersma, et al., 2017) and is a function of the surface reflectance, the NO_2 vertical profile, and scattering in the atmosphere among other factors. Using accurate and high-resolution data (spatially and temporally) as inputs in calculating the AMF can significantly reduce the overall errors of the AMF (S. Choi et al., 2019; Goldberg et al., 2017; Lamsal, 2020; Laughner, Zare, & Cohen, 2016, Laughner, Zhu, & Cohen, 2019; Lin et al., 2015; M. Liu et al., 2019; Russell, Perring, et al., 2011; Zhao et al., 2020) and thus the tropospheric vertical column content.

Operationally, the TM5-MP model ($1 \times 1°$ resolution) is used to provide the NO_2 vertical shape profile, and the climatological Lambertian Equivalent Reflectivity ($0.5 \times 0.5°$ resolution) (Kleipool et al., 2008) is used to provide the surface reflectivities. The operational AMF calculation does not explicitly account for aerosol absorption or scattering effects, which are partially accounted for in the effective cloud radiance fraction (Chimot et al., 2016). There is already some evidence that the current TROPOMI operational NO_2 product may have a low bias of 20%–40% in urban areas; much of this bias may be attributed to the AMF (Judd, Al-Saadi, Szykman, et al. 2020; Verhoelst et al., 2020). While the operational product does have larger

uncertainties in the tropospheric column contents than a product with higher spatial resolution inputs, we limit our analysis to relative trends, which dramatically reduces this uncertainty.

2.2. Re-gridding

For our analysis we re-grid the operational TROPOMI tropospheric vertical column NO_2, with native pixels of approximately 3.5×7 km^2, to a newly defined $0.01° \times 0.01°$ grid (approximately 1×1 km^2) centered over the continental United States (CONUS; corner points: SW: 24.5°N, 124.75°W; NE: 49.5°N, 66.75°W). Before re-gridding, the data are filtered so as to use only the highest quality measurements (quality assurance flag (QA_flag) > 0.75). By restricting to this QA value, we are removing mostly cloudy scenes (cloud radiance fraction > 0.5) and observations over snow-ice. Once the re-gridding has been completed, the data are averaged over varying timeframes as discussed in the results section.

2.3. Other Data sets

Additionally, we use three complementary products in some sections of our analysis. We compare tropospheric vertical column information from TROPOMI to the same quantity from the NASA OMI NO_2 version 4 product in a qualitative sense. Only OMI pixels with cloud fractions < 0.3, surface albedo < 0.3, and not affected by the "row anomaly" are included. When filtering TROPOMI data based on temperature, we use the maximum daily hourly 2-m temperature from the ERA5 re-analysis. To downscale the ERA5 re-analysis, which is provided at $0.25° \times 0.25°$, we spatially interpolate maximum daily hourly 2-m temperature to $0.01° \times 0.01°$ using bilinear interpolation. For that reason, the heat-urban island effect and any microscale meteorology features (e.g., sea breezes) will not be accounted for, but these effects should be minor for our particular analysis, which groups temperatures in ~5°C intervals.

3. Results

3.1. TROPOMI NO_2 in CONUS

Figure 1 depicts the 2019 CONUS annual average of TROPOMI and OMI tropospheric vertical column NO_2 compared to averages over monthly, weekly, and daily timeframes.

This example illustrates how shorter timeframes compare to the annual average in both magnitude and clarity. In the single daily snapshot (20 September 2019), there are wide sections that are missing due to cloud coverage. Missing data in the OMI NO_2 snapshot is much more widespread than TROPOMI due to the "row anomaly." which obstructs a portion of OMI's field of view. In the areas that do have coverage, values can be a factor of five different than the annual average, but the spatial heterogeneities are generally captured. When oversampling over a one-week period (16–22 September 2019), the TROPOMI image quickly starts to resemble the annual average with some differences in magnitude due to meteorological factors, such as temperature (which will be discussed later), but the OMI image is still very noisy. A monthly oversampled image essentially captures the same spatial heterogeneities as the annual average, but with magnitude differences due to meteorology. In most scenarios, a one-month average should be considered the minimum amount of oversampling time needed for TROPOMI to properly capture spatial heterogeneities, while for OMI ~12 months of data is needed in order to properly capture spatial heterogeneities. It should be noted that September was specifically chosen for this analysis due to its propensity to have both less cloud coverage and snow cover than other months. If oversampling during winter months (i.e., December–March), which tend to have fewer ideal conditions for satellite retrievals of trace gases, oversampling times will need to be longer to achieve similar clarity. In a qualitative sense, OMI yields larger values than TROPOMI in most areas (rural and urban alike). This is consistent with other literature, which shows OMI yielding larger values than TROPOMI (Wang et al., 2020) and a low bias in TROPOMI in U.S. urban areas (Judd, Al-Saadi, Szykman, et al., 2020).

When visually inspecting the CONUS TROPOMI NO_2 average during the initial 20 months of the TROPOMI record (1 May 2018–31 Dec 2019) (Figure 2), we now start to see clear spatial heterogeneities across the domain. The largest U.S. cities can be seen, and their magnitudes can be compared to each other (results further discussed later).

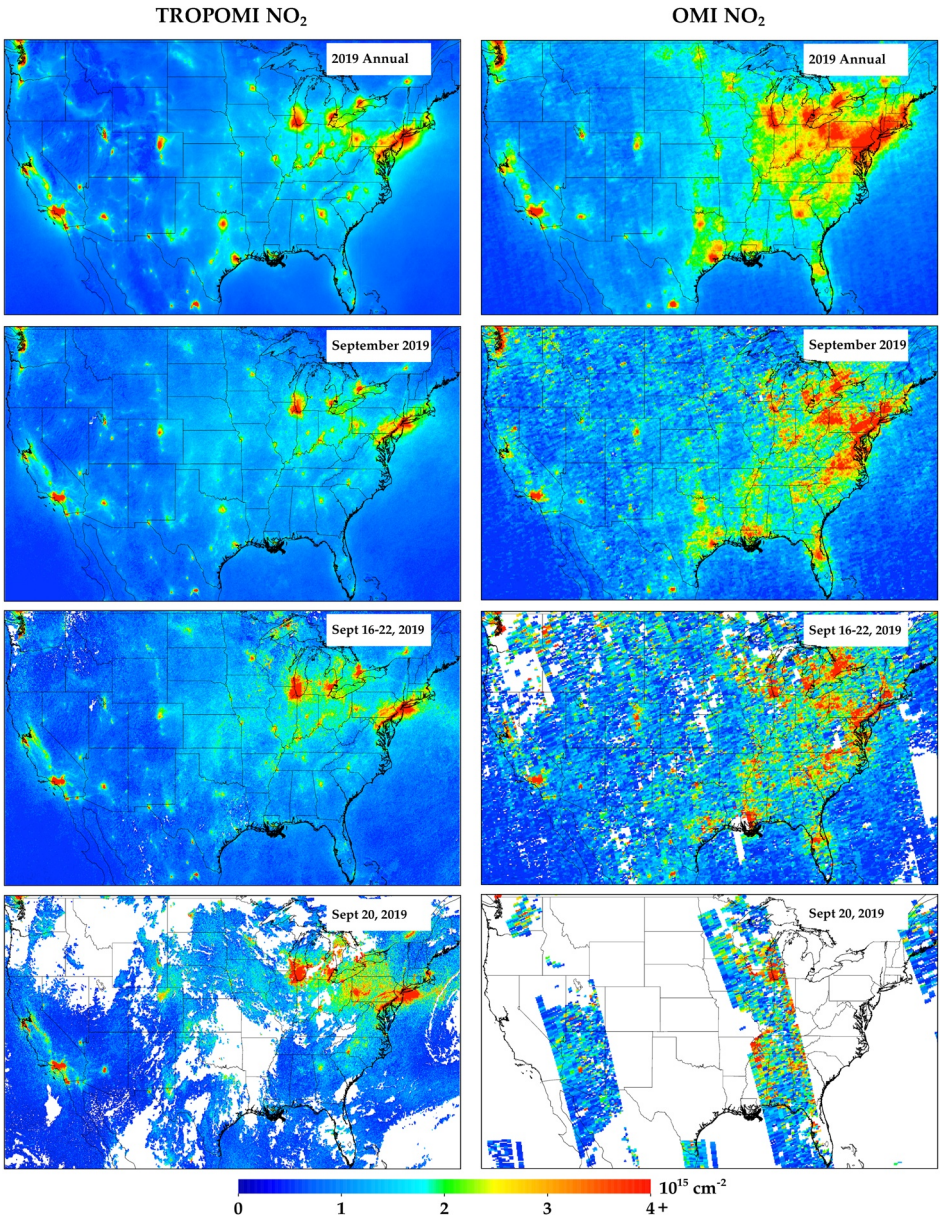

Figure 1. (Left) TROPOMI NO_2 and (right) OMI NO_2 oversampled to 0.01° × 0.01° spatial resolution for four different temporal resolutions: (top row) annual, (second row) monthly, (third row) weekly, and (bottom row) daily.

Equally important, smaller sources of NO_2 pollution can now be observed, and they are not spatially smeared into the background NO_2 concentration. For example, when magnifying the western United States (Figure 3), the roadway network and related activity in the Idaho Snake River valley can be clearly observed. Other examples are the copper mining operations in Arizona associated with the Morenci Mine and Bagdad Mine, the coal mining operations in the Powder River Basin and Green River Basin in Wyoming, and to a lesser extent the gold mining operations associated with the Goldstrike, Cortez, and Round Mountain mines in Nevada. In addition, NO_2 concentrations are clearly correlated with oil & gas operations in the Permian (Texas) and Bakken (North Dakota) basins (also discussed in Dix et al., 2020) and are > 5 times larger than the NO_2 in the rural areas upwind. Individual spikes in NO_2 associated with NO_X emissions from large power plants (e.g., Navajo, Cholla, Springerville/Coronado (S/C) in Arizona, Craig in Colorado, Colstrip in Montana, N Valmy in Nevada, Four Corners/San Juan (4C/SJ) in New Mexico, Intermountain, Bonanza, Hunter/Huntington (H/H) in Utah, Jim Bridger in Wyoming) can also be observed during this 2018–2019

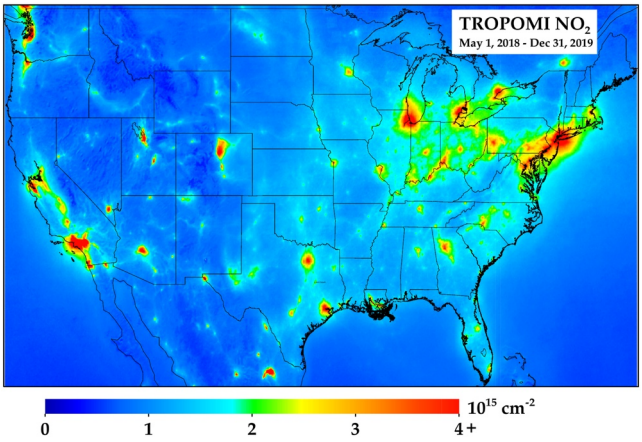

Figure 2. TROPOMI NO_2 oversampled to 0.01° × 0.01° spatial resolution during 1 May 2018–31 December 2019. Only pixels exceeding a quality assurance flag of 0.75 are included.

period even though there have been large reductions (~85%) in the NO_X emissions from most of these power plants since the introduction of the federally mandated NO_X SIP call in 2003.

TROPOMI data are especially powerful in analyzing local variations in NO_2 pollution as compared to predecessor instruments. In Figure 4, we zoom into five different U.S. states, and in Table 1 we provide the largest NO_2 values in each state; note that in Figure 4 we use a colorbar that is not linear in order to better differentiate urban versus rural values.

In Figure 5, we zoom into six different U.S. cities. In each instance, the oversampled TROPOMI NO_2 images exhibit features that match known NO_X emissions patterns. The larger NO_2 values correlate very well to the interstate network, population density, and industrial activity hubs (such as manufacturing facilities, airports, and shipping ports). For example, in the image of Maryland, the largest value is observed at the Baltimore Harbor, which is a confluence of several major highways, a large shipping port, the city incinerator, and many industrial facilities. Similarly, the largest values in Chicago exist along the I-55 corridor which has a high traffic volume and a high-density of industrial facilities, with secondary maxima at the O'Hare International airport and the U.S. Steel Corp operations in East Chicago, Indiana. In Los Angeles, the spatial pattern matches the basin outline very well, with the largest values between downtown Los Angeles and the Long Beach Shipping Port. In Houston, Texas the largest values are nearest to the petrochemical refining facilities east of town. For all cases, TROPOMI can accurately quantify the relative relationship between the largest sources of NO_X emissions and NO_2 concentrations.

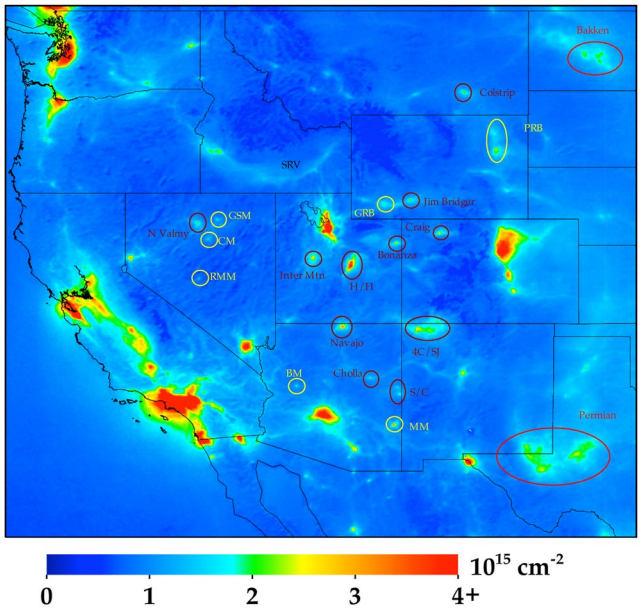

Figure 3. Same data shown in Figure 2, but now zoomed into the western United States. Power plants are outlined in dark magenta, mining operations in yellow, and oil & gas in bright red.

3.2. Day-of-the-Week Relationships

A common use of oversampled satellite data is in investigating the weekly cycle of NO_X emissions. In Figure 6, we show the weekly pattern of NO_2 across CONUS for three different days of the week as well as the full weekly cycle in seven U.S. cities; we selected U.S. metropolitan areas that were both large and representative of geographic diversity. In all cities, the NO_2 appears to be approximately equivalent amongst all weekdays with some minor exceptions. NO_2 pollution is 2.5% larger on Tuesday than a typical weekday, while Mondays and Fridays have 1.4% and 1.3% lower NO_2 pollution than a typical weekday. On Saturdays, NO_2 is 16% lower than the weekday averages, and on Sundays 24% lower. Standard errors of the mean for each city are shown in Table S1, and are approximately 10% for any given city, and approximately 4% when all cities are aggregated together. This means that NO_2 changes on weekends—including the differences between Saturdays and Sundays—are statistically significant, but the difference between weekdays are not yet statistically significant. As more TROPOMI NO_2 data are acquired over time, these standard errors of the mean will decrease, and we might be able to deduce statistically significant changes between individual weekdays. The weekend changes calculated here (16% drop on Saturdays, 24% drop on Sundays) are less dramatic than previously reported weekend changes (30%–60% drops) in the 2005–2013 timeframe (de Foy, Lu, & Streets, 2016; Russell, Valin, et al., 2010; Valin et al., 2014). There are two explanations for the flattening of the weekday-weekend cycle: 1.) as overall emissions are decreasing, the NO_2 lifetime in many cities is increasing (Stavrakou, Müller, Bauwens, et al., 2020) and 2.) passenger vehicles, which have a

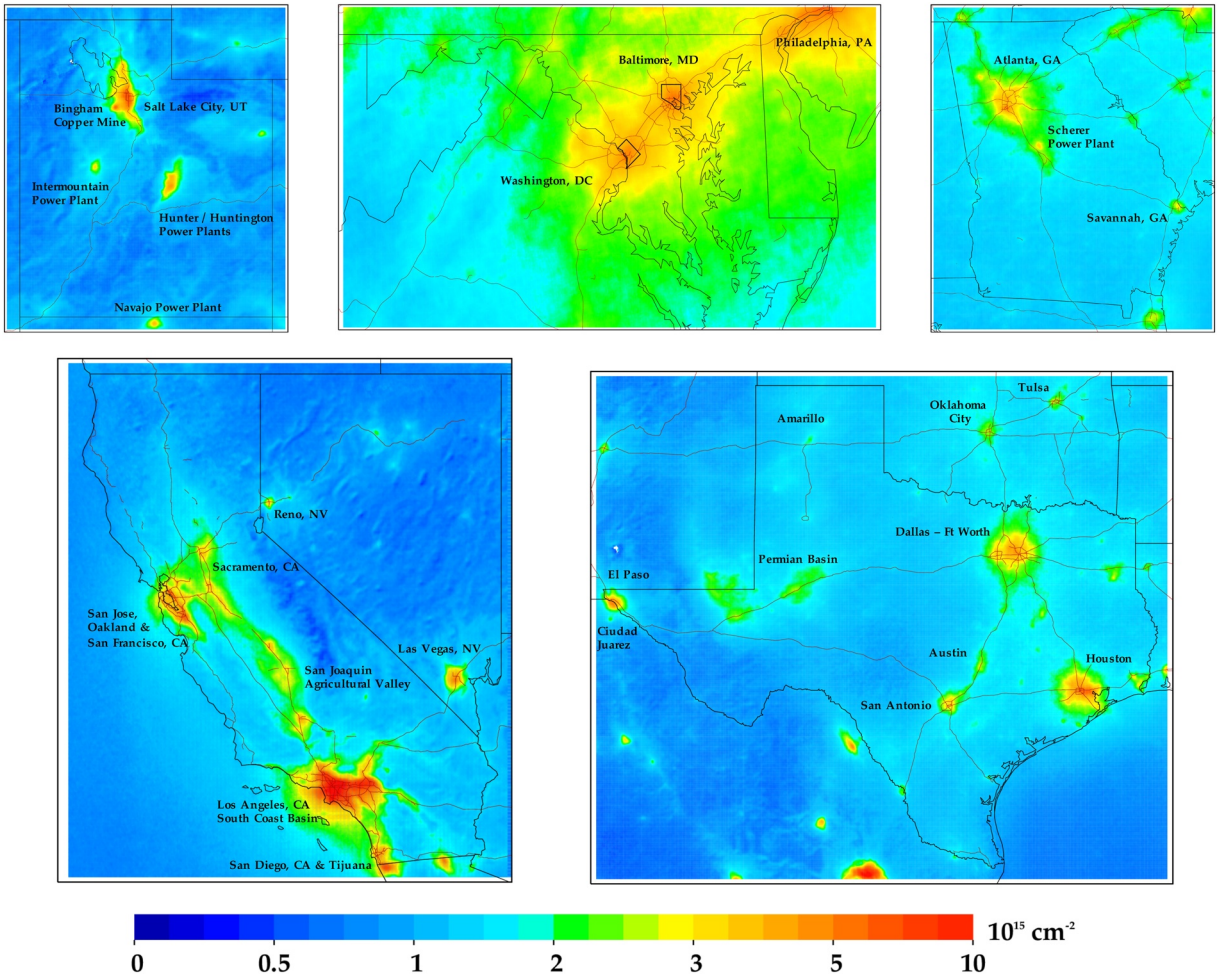

Figure 4. Same data shown in Figure 2, but now zoomed into five different U.S. states. Color bar has been adjusted to better differentiate spatial heterogeneities on a local scale.

pronounced weekday-weekend emissions pattern, are continually representing a smaller fraction of NO_X emissions over time (Dallmann & Harley, 2010; McDonald et al., 2012).

When analyzing the weekday/weekend differences, there should be some consideration for the difference in traffic patterns and general activity between weekends and weekdays. On weekends, traffic counts generally peak in the early afternoon, while on weekdays traffic counts peak in the evening, with a secondary peak in the early morning (de Foy, 2018). Since the satellite observation is acquired in the early afternoon, we suggest that the 24-h averaged NO_X emissions difference between weekdays and weekends may be even greater than implied by the satellite data. The soon-to-be-launched TEMPO instrument, a geostationary satellite, will hopefully be able to better quantify the morning and evening differences of NO_X emissions (Chance et al., 2019; Penn & Holloway, 2020; Zoogman et al., 2017).

3.3. Hot Versus Warm Days

In Figure 7, we show the variation in column NO_2 as a function of the daily maximum 2-m temperature. Due to varying climates across the United States, most cities do not have values for all temperature bins. In general, as temperatures increase, NO_2 decreases; this is primarily driven by $j(NO_2)$ which increases with stronger sunlight. When temperatures are >32°C, we observe a leveling with increasing temperature. This may be related to increasing anthropogenic NO_X emissions (Abel et al., 2017; He et al., 2013) at high temperatures despite a shorter NO_2 lifetime. This may also be driven by biogenic or natural causes, such as

Table 1
Largest NO_2 Column Value in Each U.S. State During the 1 May 2018–31 Dec 2019 Period

U.S. state	Latitude (°N)	Longitude (°E)	NO2 (molec/cm2)	Detailed location
CA	34.03	−118.18	1.41E+16	E Los Angeles, CA
NY	40.72	−73.97	1.13E+16	East River, Brooklyn, NY
NJ	40.69	−74.14	9.75E+15	Port Newark, NJ
IL	41.82	−87.77	7.31E+15	Cicero, Chicago, IL (near MDW)
WA	47.46	−122.26	6.90E+15	Tukwila, WA (SE Seatle)
IN	41.66	−87.47	6.28E+15	E Chicago, IN (Steel Mill)
UT	40.71	−111.9	6.18E+15	S Salt Lake City, UT
CO	39.76	−105.02	5.98E+15	Highland, Denver, CO
PA	39.95	−75.16	5.95E+15	Downtown Philadelphia, PA
AZ	33.47	−112.15	5.87E+15	Cuatro Palmas, Phoenix, AZ
MI	42.31	−83.11	5.74E+15	Detroit, MI
TX	29.74	−95.14	5.58E+15	Deer Park, Houston, TX
CT	41	−73.67	5.46E+15	Greenwich, CT
NV	36.1	−115.18	4.97E+15	Las Vegas Strip, Las Vegas, NV
MD	39.28	−76.6	4.94E+15	Port of Baltimore, Baltimore, MD
DC	38.89	−77.01	4.65E+15	Capitol Hill, Washington, DC
GA	33.64	−84.42	4.65E+15	Hartsfield Airport, Atlanta, GA
VA	38.88	−77.05	4.59E+15	Pentagon, Arlington, VA
DE	39.8	−75.37	4.34E+15	Claymont, Wilmington, DE
OR	45.52	−122.65	4.25E+15	Buckman, Portland, OR
KY	38.18	−85.73	4.21E+15	Louisville, KY (Airport)
OH	39.12	−84.54	4.20E+15	Cincinnati, OH
MA	42.37	−71.06	4.14E+15	Charlestown, Boston, MA (near BOS)
LA	29.93	−90.14	3.98E+15	Mississippi River, New Orleans, LA
NC	35.24	−80.85	3.76E+15	Catawba, NC (near Marshall Steam PP)
WV	38.94	−82.11	3.68E+15	Lakin, WV (near Gavin PP)
MO	38.68	−90.19	3.67E+15	Mississippi River, St Louis, MO
KS	39.12	−94.6	3.61E+15	Missouri River, Kansas City, KS
TN	36.16	−86.77	3.52E+15	Nashville, TN
FL	25.85	−80.34	3.40E+15	Medley, Miami, FL
WI	42.86	−87.82	3.40E+15	Oak Creek, WI (near Oak Creek PP)
MN	44.97	−93.24	3.28E+15	Mississippi River, Minneapolis, MN
AL	33.52	−86.82	3.21E+15	Fountain Heights, Birmingham, AL
RI	41.8	−71.41	2.88E+15	S Providence, RI
IA	41.25	−95.88	2.79E+15	Council Bluffs, IA
NE	41.25	−95.88	2.79E+15	Missouri River, Omaha, NE
OK	36.16	−96	2.64E+15	Tulsa, OK
WY	43.69	−105.32	2.52E+15	Thunder Basin Coal, WY
SC	32.88	−79.99	2.52E+15	N Charleston, SC
NM	35.11	−106.62	2.51E+15	Albuquerque, NM
AR	35.12	−90.1	2.46E+15	W Memphis, AR
ID	43.58	−116.23	2.30E+15	Boise, ID (Airport)
ND	47.35	−101.81	2.24E+15	Beulah, ND (near Dakota Gasification Co)

Table 1
Continued

U.S. state	Latitude (°N)	Longitude (°E)	NO2 (molec/cm2)	Detailed location
MT	45.86	−106.57	2.20E+15	Colstrip, MT (near Colstrip PP)
NH	42.94	−70.81	1.93E+15	Hampton, NH
ME	43.66	−70.29	1.90E+15	Portland, ME
MS	32.34	−90.19	1.77E+15	Jackson, MS
SD	43.6	−96.74	1.53E+15	N Sioux Falls, SD
VT	42.91	−73.18	1.49E+15	Wilmington, VT

Note. Ordered by largest to smallest maximum value.

the faster dissociation of peroxy-acyl nitrates (PANs) or increased soil NO_X emissions (Rasool et al., 2019; Romer et al., 2018) at hot temperatures. The latter reasons are likely causing rural areas to observe increases in NO_2 as temperatures warm above 32°C. The temperature-driven stabilization of NO_2 at very high temperatures appears to hold for all cities except Chicago. Standard errors of the mean for each city are shown in Table S2, and are approximately 7% for any given city on warm/hot temperature days (>20°C), and approximately 2%–3% when all cities are aggregated together. This means that the NO_2 decreases with increasing temperature as well as the NO_2 increases on the hottest days are statistically significant in most areas. It should be noted that there are cross-correlations with increased temperature such as a lower solar zenith angle (which affects photolysis rates of chemical species and the satellite viewing geometry), larger biogenic volatile organic compound (BVOC) emissions in forested areas (which affects the NO_2 lifetime), and higher total water columns (which affects wet deposition and introduces an increased spectral interference). Apportionment of the effects of natural versus anthropogenic sources contributing to NO_2 increases in urban areas on the hottest days will be the subject of future research using model simulations.

3.4. Relationship With Surface NO_2 Concentrations

To understand how well TROPOMI NO_2, without any adjustment, captures surface-level concentrations, we compare the 2019 annual TROPOMI NO_2 average to 24-h annual average EPA AQS monitor data. The surface-level concentrations from the EPA AQS network are known to have a high instrument bias (Dickerson et al., 2019) and thus referred to as NO_2* hereafter. In Figure 8, we show a scatterplot between 2019 annual averages of oversampled TROPOMI NO_2 and AQS surface-level NO_2* concentrations. For our analysis, we restrict our fit to monitoring sites that are not "near-road." The EPA requests certain states to site "near-road" NO_2 monitors, which are requested to be within 20 m of a major highway; we do not expect TROPOMI observations to capture this very fine spatial gradient, and are therefore not considered in our fit. Figure 8 demonstrates that there is a strong correlation ($R^2 = 0.66$) between a linear fit and monitoring sites considered to be "not near-road." which suggests that many (but not all) of the spatial heterogeneities observed by TROPOMI over long time intervals (e.g., year) are real and not an artifact of the processing algorithms. We are encouraged to see that a simple linear fit is able to capture near-surface NO_2 variability well. In order to better estimate surface-level concentrations, TROPOMI NO_2 data should be merged with a model simulation (Cooper, Martin, McLinden, & Brook, 2020) and/or land-use characteristics (Bechle et al., 2015; Beloconi & Vounatsou, 2020; Di et al., 2019; Larkin et al., 2017).

4. Conclusions

This study investigates the capabilities of the TROPOMI in observing the spatial and temporal patterns of NO_2 pollution in the continental United States (CONUS). Here, we demonstrate that TROPOMI can capture fine-scale spatial heterogeneities in urban areas, such as emissions related to airport/shipping operations and high traffic; this type of spatial precision cannot be matched by predecessor satellite instruments over short timescales (<1 year). We find that Saturday and Sunday concentrations are 16% and 24% lower respectively than during weekdays, with the caveat that diurnal emissions patterns vary among weekdays and weekends. We also analyze the effects of hot temperatures (>32°C) on NO_2 column amounts and find

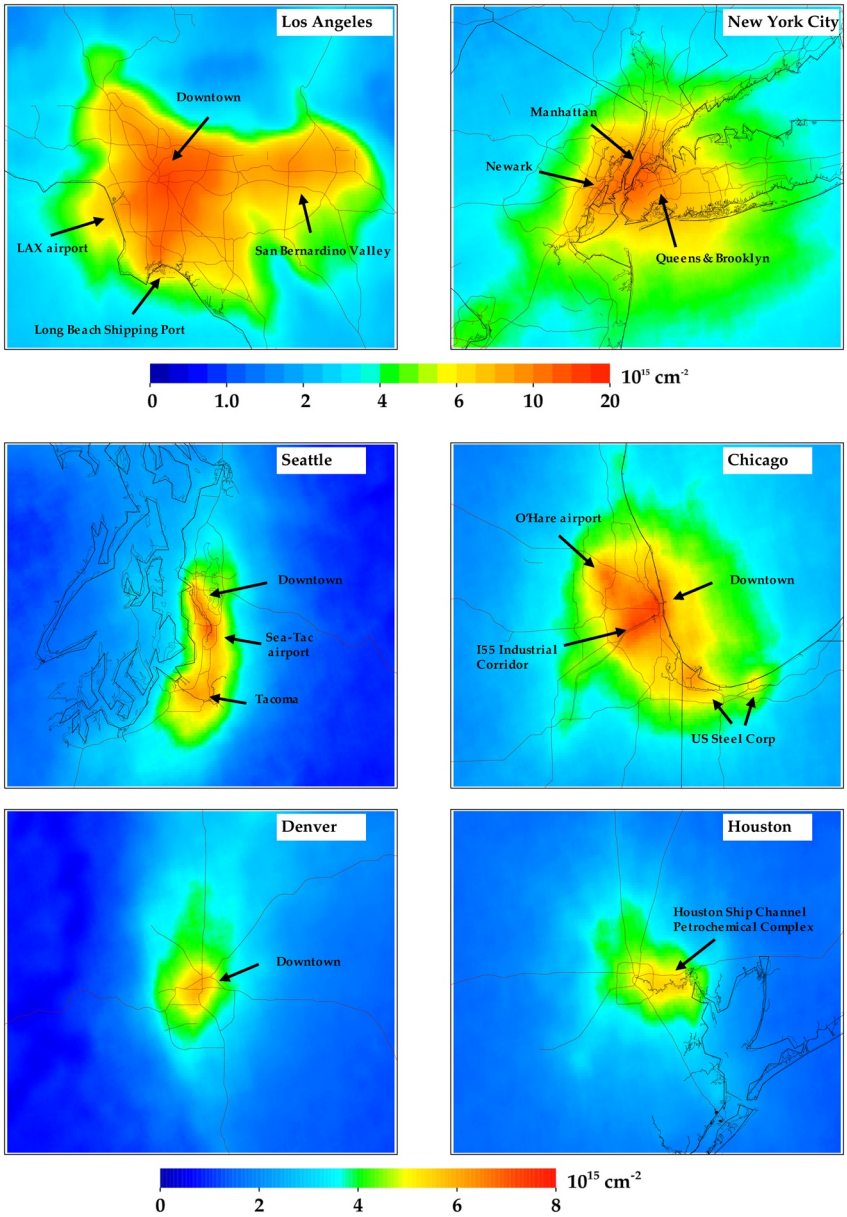

Figure 5. Same data shown in Figure 2, but now zoomed into six different U.S. cities. Color bar has been adjusted to better differentiate spatial heterogeneities on a local scale.

that column NO_2 is generally larger on the hottest days as compared to warm days (26°C–32°C). Finally, we compare column NO_2 with surface-level NO_2 estimates and find relatively good correlation ($R^2 = 0.66$).

For this work, we rely on the operational TROPOMI NO_2 algorithm, which underestimates tropospheric vertical column NO_2 in urban areas. Previous studies suggest that this underestimate is due to the AMF and ~5km pixel size which cannot resolve street-level variations in concentrations (Goldberg, Lu, Streets, et al., 2019; Griffin et al., 2019; Judd, Al-Saadi, Szykman, et al., 2020; Judd, Al-Saadi, Janz, et al., 2019; Zhao et al., 2020); investigating the effects of the AMF bias on trends as well as investigating the effects of the pixels sizes will be the subject of future work. Also, there may be a clear-sky bias (Geddes, Murphy, et al., 2012) associated with any satellite retrieval, but the general spatial heterogeneities of NO_2 pollution should be similar amongst all types of weather conditions when averaged over long timeframes. Lastly, interpreting results from polar-orbiting satellite instruments, such as TROPOMI, should be made with some caution due to the mid-day only data collection time. Work quantifying this bias has shown

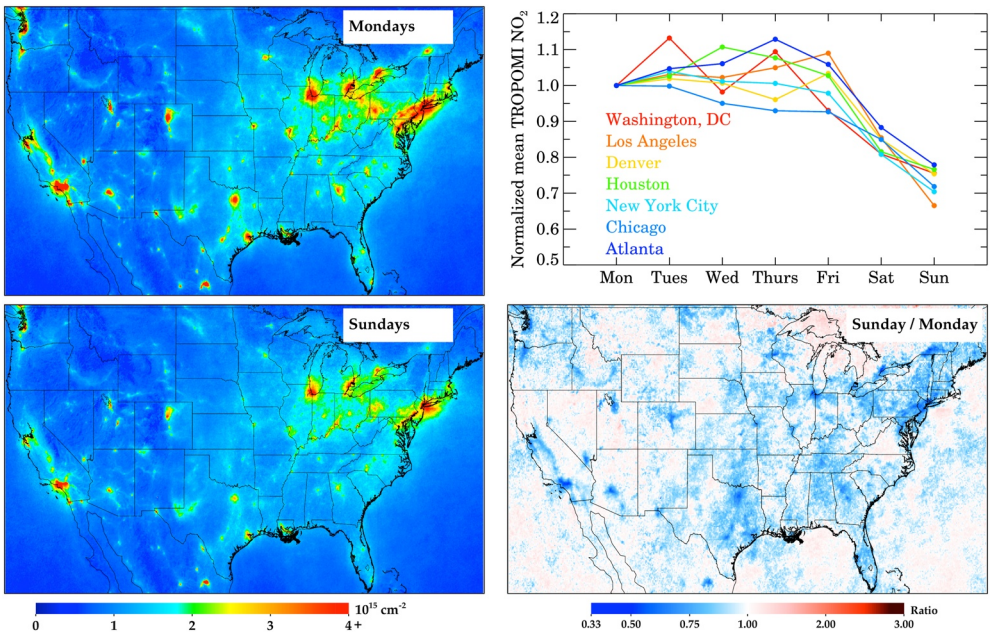

Figure 6. Weekly variations in column NO_2. (Top left) TROPOMI NO_2 during Mondays. (Bottom left) TROPOMI NO_2 during Sundays. (Top right) Weekly variation of TROPOMI NO_2 in seven U.S. cities normalized to Mondays; city averages are across a 1° × 1° box centered on the city. (Bottom right) Ratio between Sundays and Mondays.

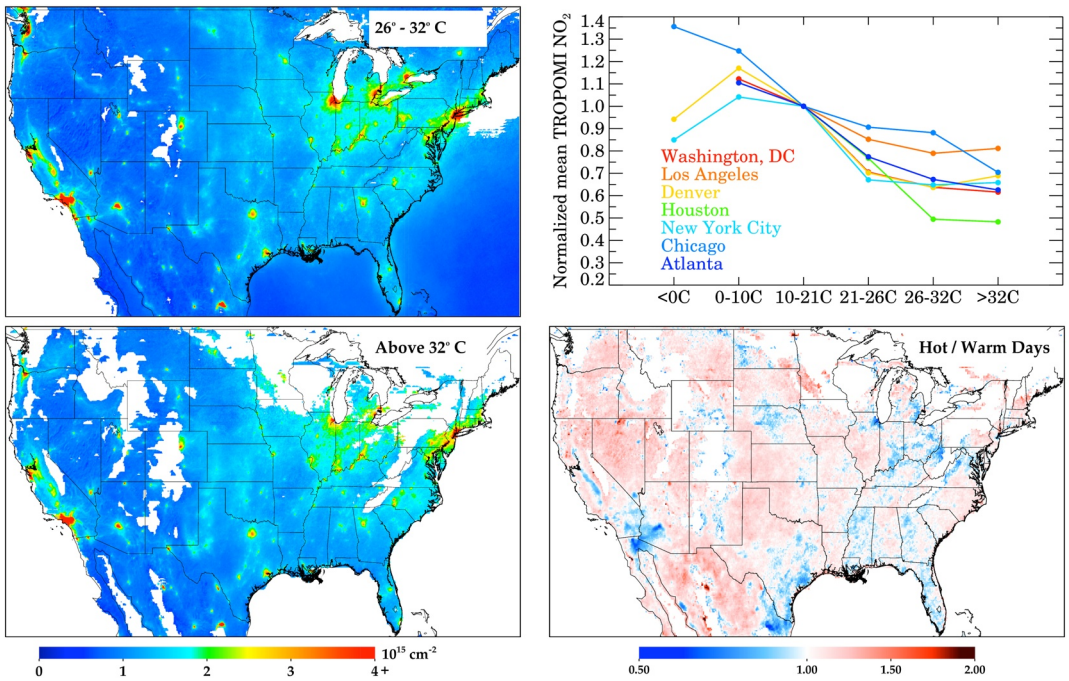

Figure 7. Temperature variations in column NO_2. (Top left) TROPOMI NO_2 when maximum daily 2-m temperature is between 26°C–32°C (Warm; 80°F–90°F); only areas where >10 valid pixels are shown. (Bottom left) TROPOMI NO_2 when maximum daily 2-m temperature is greater than 32°C (hot; 90°F); only areas where >10 valid pixels are shown. (Top right) Temperature variation of TROPOMI NO_2 in seven U.S. cities normalized to 10°C–21°C (50°F–70°F); city averages are across a 1° × 1° box centered on the city. (Bottom right) Ratio between days with daily 2-m temperature >32°C (Hot) and 26°C–32°C (Warm).

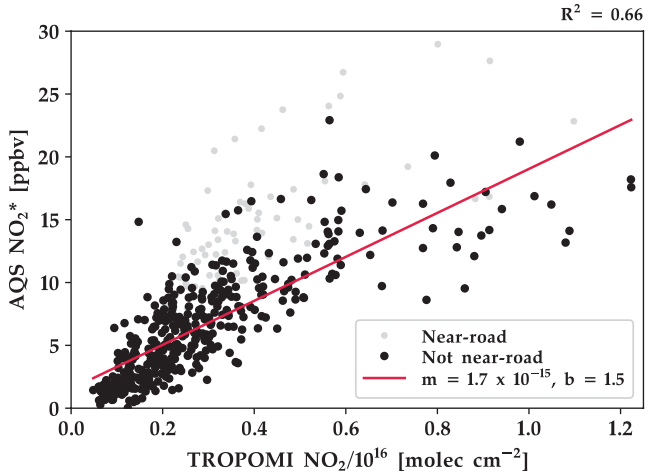

Figure 8. EPA AQS annual surface NO_2* observations for 2019 compared to the collocated oversampled 0.01° × 0.01° TROPOMI value during the same timeframe. R^2 represents the correlation between TROPOMI and not near-road monitors.

that NO_2 column measurements are lower and incrementally more spatially homogeneous in the afternoon than during the morning (Chong et al., 2018; Fishman et al., 2008; Herman et al., 2019; Knepp et al., 2015; Penn & Holloway, 2020; Tzortziou et al., 2015); it is likely that data from geostationary platforms such as TEMPO (Zoogman et al., 2017), GEMS (W. J. Choi, 2018), and Sentinel 4 (Timmermans et al., 2019), will be able to provide further insight on this time-of-day bias.

Because TROPOMI can observe and measure NO_2 increases attributed to relatively small sources, future work should be able to quantify emissions from small sources (e.g., industrial activities, ship plumes, small wildfires) that had previously gone undetected from predecessor space-based instruments. Furthermore, due to the instrument's excellent stability, precision, and spatial resolution, it is no longer necessary to average over 6+ months of data to gain a clear depiction of regional NO_2 abundances; instead monthly, weekly or even daily aggregations could suffice for many purposes. The examples presented here demonstrate how TROPOMI NO_2 satellite data can be advantageous for policymakers requesting information at high spatial resolution and short timescales, in order to assess, devise, and evaluate regulations. Future health impact assessment studies can use the high-spatial resolution capabilities of TROPOMI NO_2 to investigate disparities in traffic-related air pollution exposure and associated health effects between neighborhoods and population sub-groups within cities.

Data Availability Statement

TROPOMI NO_2 data can be freely downloaded from the European Space Agency Copernicus Open Access Hub or the NASA EarthData Portal (http://doi.org/10.5270/S5P-s4ljg54). ERA5 can be freely downloaded from the Copernicus Climate Change (C3S) climate data store (CDS) (https://cds.climate.copernicus.eu/#!/search?text=ERA5&type=dataset).

Acknowledgments
This work has been supported by the Department of Energy, Office of Fossil Energy. This work has also been sponsored by a Health and Air Quality (HAQ) grant (award #: 80NSSC19K0193), and two Atmospheric Composition Modeling and Analysis Program grants (award #: 80NSSC17K0280 and 80NSSC19K0946). We would also like to acknowledge valuable comments during the manuscript preparation from Joel Dreessen of Maryland Department of the Environment. The submitted manuscript has been created by UChicago Argonne, LLC, Operator of Argonne National Laboratory ("Argonne"). Argonne, a US Department of Energy Office of Science laboratory, is operated under contract no. DE-AC02-06CH11357.

References

Abel, D. W., Holloway, T., Kladar, R. M., Meier, P., Ahl, D., Harkey, M., & Patz, J. (2017). Response of power plant emissions to ambient temperature in the Eastern United States. *Environmental Science and Technology*, *51*(10), 5838–5846. https://doi.org/10.1021/acs.est.6b06201

Achakulwisut, P., Brauer, M., Hystad, P., & Anenberg, S. C. (2019). Global, national, and urban burdens of paediatric asthma incidence attributable to ambient NO_2 pollution: estimates from global datasets. *Lancet Planet Health*, *3*(4), e166–e178. https://doi.org/10.1016/S2542-5196(19)30046-4

Anenberg, S. C., Henze, D. K., Tinney, V., Kinney, P. L., Raich, W., Fann, N., et al. (2018). Estimates of the global burden of ambient PM2.5, ozone, and NO2 on asthma incidence and emergency room visits. *Environmental Health Perspectives*, *126*(10), 107004. https://doi.org/10.1289/EHP3766

Bechle, M. J., Millet, D. B., & Marshall, J. D. (2015). National spatiotemporal exposure surface for NO2: Monthly scaling of a satellite-derived land-use regression, 2000-2010. *Environmental Science and Technology*, *49*(20), 12297–12305. https://doi.org/10.1021/acs.est.5b02882

Beirle, S., Boersma, K. F., Platt, U., Lawrence, M. G., & Wagner, T. (2011). Megacity emissions and lifetimes of nitrogen oxides probed from space. *Science*, *333*(6050), 1737–1739. https://doi.org/10.1126/science.1207824

Beirle, S., Borger, C., Dörner, S., Li, A., Hu, Z., Liu, F., et al. (2019). Pinpointing nitrogen oxide emissions from space. *Science Advances*, *5*(11), eaax9800. https://doi.org/10.1126/sciadv.aax9800

Beirle, S., Platt, U., Wenig, M., & Wagner, T. (2003). Weekly cycle of NO2 by GOME measurements: A signature of anthropogenic sources. *Atmospheric Chemistry and Physics*, *3*(6), 2225–2232. https://doi.org/10.5194/acp-3-2225-2003

Bell, M. L. (2004). Ozone and short-term mortality in 95 US urban communities, 1987-2000. *JAMA*, *292*(19), 2372. https://doi.org/10.1001/jama.292.19.2372

Bell, M. L., Peng, R. D., & Dominici, F. (2006). The exposure-response curve for ozone and risk of mortality and the adequacy of current ozone regulations. *Environmental Health Perspectives*, *114*(4), 532–536. https://doi.org/10.1289/ehp.8816

Beloconi, A., & Vounatsou, P. (2020). Bayesian geostatistical modelling of high-resolution NO2 exposure in Europe combining data from monitors, satellites and chemical transport models. *Environment International*, *138*, 105578. https://doi.org/10.1016/j.envint.2020.105578

Boersma, K. F., Eskes, H. J., & Brinksma, E. J. (2004). Error analysis for tropospheric NO2 retrieval from space. *Journal of Geophysical Research*, *109*(D4). https://doi.org/10.1029/2003JD003962

Boersma, K. F., Eskes, H. J., Richter, A., De Smedt, I., Lorente, A., Beirle, S., et al. (2018). Improving algorithms and uncertainty estimates for satellite NO2 retrievals: results from the quality assurance for the essential climate variables (QA4ECV) project. *Atmospheric Measurement Techniques*, *11*(12), 6651–6678. https://doi.org/10.5194/amt-11-6651-2018

Bovensmann, H., Burrows, J. P., Buchwitz, M., Frerick, J., Noël, S., Rozanov, V. V., et al. (1999). SCIAMACHY: Mission objectives and measurement modes. *Journal of the Atmospheric Sciences*, *56*(2), 127–150. https://doi.org/10.1175/1520-0469(1999)056<0127:SMOAMM>2.0.CO;2

Broeckaert, F., Arsalane, K., Hermans, C., Bergamaschi, E., Brustolin, A., Mutti, A., & Bernard, A. (1999). Lung epithelial damage at low concentrations of ambient ozone. *Lancet*, *353*(9156), 900–901. https://doi.org/10.1016/S0140-6736(99)00540-1

Burnett, R. T., Stieb, D., Brook, J. R., Cakmak, S., Dales, R., Raizenne, M., et al. (2004). Associations between short-term changes in nitrogen dioxide and mortality in Canadian cities. *Archives of Environmental Health*, *59*(5), 228–236. https://doi.org/10.3200/AEOH.59.5.228-236

Burns, D. A., Gay, D. A., & Lehmann, C. M. B. (2016). Acid rain and its environmental effects: Recent scientific advances. *Atmospheric Environment*, *146*, 1–4. https://doi.org/10.1016/J.ATMOSENV.2016.10.019

Burrows, J. P., Weber, M., Buchwitz, M., Rozanov, V., Ladstatter-Weibenmayer, A., Richter, A., et al. (1999). The global ozone monitoring experiment (GOME): Mission concept and first scientific results. *Journal of Atmospheric Sciences*, *56*, 151–175. https://doi.org/10.1175/1520-0469(1999)056<0151:TGOMEG>2.0.CO;2

Canty, T. P., Hembeck, L., Vinciguerra, T. P., Anderson, D. C., Goldberg, D. L., Carpenter, S. F., et al. (2015). Ozone and NO_x chemistry in the eastern US: Evaluation of –AQ/CB05 with satellite (OMI) data. *Atmospheric Chemistry and Physics*, *15*(19), 10965–10982. https://doi.org/10.5194/acp-15-10965-2015

Castellanos, P., & Boersma, K. F. (2012). Reductions in nitrogen oxides over Europe driven by environmental policy and economic recession. *Scientific Reports*, *2*(2), 1–7. https://doi.org/10.1038/srep00265

Chance, K., Liu, X., Miller, C. C., González Abad, G., Huang, G., Nowlan, C., et al. (2019). TEMPo green paper: Chemistry, physics, and meteorology experiments with the tropospheric emissions: Monitoring of pollution instrument. In S. P. Neeck, T. Kimura, & P. Martimort (Eds.), Sensors, systems, and next-generation satellites XXIII (Vol. 11151, p. 10). SPIE. https://doi.org/10.1117/12.2534883

Chimot, J., Vlemmix, T., Veefkind, J. P., De Haan, J. F., & Levelt, P. F. (2016). Impact of aerosols on the OMI tropospheric NO2 retrievals over industrialized regions: How accurate is the aerosol correction of cloud-free scenes via a simple cloud model? *Atmospheric Measurement Techniques*, *9*(2), 359–382. https://doi.org/10.5194/amt-9-359-2016

Choi, S., Lamsal, L. N., Follette-Cook, M., Joiner, J., Krotkov, N. A., Swartz, W. H., et al. (2019). *Assessment of NO2 observations during DISCOVER-AQ and KORUS-AQ field campaigns*. AMTD. https://doi.org/10.5194/amt-2019-338

Choi, W. J. (2018). Introducing the geostationary environment monitoring spectrometer. *Journal of Applied Remote Sensing*, *12*(04), 1. https://doi.org/10.1117/1.JRS.12.044005

Chong, H., Lee, H., Koo, J. H., Kim, J., Jeong, U., Kim, W., et al. (2018). Regional characteristics of NO2 column densities from pandora observations during the MAPS-Seoul campaign. *Aerosol and Air Quality Research*, *18*(9), 2207–2219. https://doi.org/10.4209/aaqr.2017.09.0341

Cohen, A. J., Brauer, M., Burnett, R. T., Anderson, H. R., Frostad, J., Estep, K., et al. (2017). Estimates and 25-year trends of the global burden of disease attributable to ambient air pollution: an analysis of data from the Global Burden of Diseases Study 2015. *The Lancet*, *389*(10082), 1907–1918. https://doi.org/10.1016/S0140-6736(17)30505-6

Cooper, M. J., Martin, R. V., McLinden, C. A., & Brook, J. R. (2020). Inferring ground-level nitrogen dioxide concentrations at fine spatial resolution applied to the TROPOMI satellite instrument. *Environmental Research Letters*, *15*, 104013. https://doi.org/10.1088/1748-9326/aba3a5

Cooper, M. J., Martin, R. V., Padmanabhan, A., & Henze, D. K. (2017). Comparing mass balance and adjoint methods for inverse modeling of nitrogen dioxide columns for global nitrogen oxide emissions. *Journal of Geophysical Research*, *122*(8), 4718–4734. https://doi.org/10.1002/2016JD025985

de Foy, B. (2018). City-level variations in NOx emissions derived from hourly monitoring data in Chicago. *Atmospheric Environment*, *176*, 128–139. https://doi.org/10.1016/j.atmosenv.2017.12.028

de Foy, B., Lu, Z., & Streets, D. G. (2016). Impacts of control strategies, the Great Recession and weekday variations on NO2 columns above North American cities. *Atmospheric Environment*, *138*(2), 74–86. https://doi.org/10.1016/j.atmosenv.2016.04.038

de Foy, B., Lu, Z., Streets, D. G., Lamsal, L. N., & Duncan, B. N. (2015). Estimates of power plant NOx emissions and lifetimes from OMI NO2 satellite retrievals. *Atmospheric Environment*, *116*(2), 1–11. https://doi.org/10.1016/j.atmosenv.2015.05.056

de Foy, B., Wilkins, J. L., Lu, Z., Streets, D. G., & Duncan, B. N. (2014). Model evaluation of methods for estimating surface emissions and chemical lifetimes from satellite data. *Atmospheric Environment*, *98*, 66–77. https://doi.org/10.1016/j.atmosenv.2014.08.051

de Gouw, J. A., Veefkind, J. P., Roosenbrand, E., Dix, B., Lin, J. C., Landgraf, J., & Levelt, P. F. (2020). Daily satellite observations of methane from oil and gas production regions in the United States. *Scientific Reports*, *10*(1), 1379. https://doi.org/10.1038/s41598-020-57678-4

Dallmann, T. R., & Harley, R. A. (2010). Evaluation of mobile source emission trends in the United States. *Journal of Geophysical Research*, *115*(D14), D14305. https://doi.org/10.1029/2010JD013862

Di, Q., Amini, H., Shi, L., Kloog, I., Silvern, R. F., Kelly, J. T., et al. (2019). Assessing NO2 concentration and model uncertainty with high spatiotemporal resolution across the contiguous united states using ensemble model averaging. *Environmental Science & Technology*, *54*, 1372–1384. https://doi.org/10.1021/acs.est.9b03358

Dickerson, R. R., Anderson, D. C., & Ren, X. (2019). On the use of data from commercial NOx analyzers for air pollution studies. *Atmospheric Environment*, *214*, 116873. https://doi.org/10.1016/j.atmosenv.2019.116873

Dix, B., Bruin, J., Roosenbrand, E., Vlemmix, T., Francoeur, C., Gorchov-Negron, A., et al. (2020). Nitrogen oxide emissions from U.S. oil and gas production: Recent trends and source attribution. *Geophysical Research Letters*, *47*(1), 2019GL085866. https://doi.org/10.1029/2019GL085866

Duncan, B. N., Lamsal, L. N., Thompson, A. M., Yoshida, Y., Lu, Z., Streets, D. G., et al. (2016). A space-based, high-resolution view of notable changes in urban NOx pollution around the world (2005-2014). *Journal of Geophysical Research: Atmosphere*, *121*(2), 976–996. https://doi.org/10.1002/2015JD024121

Elissavet Koukouli, M., Theys, N., Ding, J., Zyrichidou, I., Mijling, B., Balis, D., & Johannes Van Der A, R. (2018). Updated SO2 emission estimates over China using OMI/Aura observations. *Atmospheric Measurement Techniques*, *11*(3), 1817–1832. https://doi.org/10.5194/amt-11-1817-2018

Fishman, J., Bowman, K. W., Burrows, J. P., Richter, A., Chance, K. V., Edwards, D. P., et al. (2008). Remote sensing of tropospheric pollution from space. *Bulletin of the American Meteorological Society*, *89*(6), 805–822. https://doi.org/10.1175/2008BAMS2526.1

Geddes, J. A., Martin, R. V., Boys, B. L., & van Donkelaar, A. (2016). Long-Term trends worldwide in ambient NO 2 concentrations inferred from satellite observations. *Environmental Health Perspectives*, *124*(3), 281–289. https://doi.org/10.1289/ehp.1409567

Geddes, J. A., Murphy, J. G., O'Brien, J. M., & Celarier, E. A. (2012). Biases in long-term NO2 averages inferred from satellite observations due to cloud selection criteria. *Remote Sensing of Environment*, *124*(2), 210–216. https://doi.org/10.1016/j.rse.2012.05.008

Georgoulias, A. K., van der A, R. J., Stammes, P., Boersma, K. F., & Eskes, H. J. (2019). Trends and trend reversal detection in 2 decades of tropospheric NO2 satellite observations. *Atmospheric Chemistry and Physics*, *19*(9), 6269–6294. https://doi.org/10.5194/acp-19-6269-2019

Goldberg, D. L., Lamsal, L. N., Loughner, C. P., Swartz, W. H., Lu, Z., & Streets, D. G. (2017). A high-resolution and observationally constrained OMI NO2 satellite retrieval. *Atmospheric Chemistry and Physics*, *17*(18), 11403–11421. https://doi.org/10.5194/acp-17-11403-2017

Goldberg, D. L., Lu, Z., Oda, T., Lamsal, L. N., Liu, F., Griffin, D., et al. (2019). Exploiting OMI NO2 satellite observations to infer fossil-fuel CO2 emissions from U.S. megacities. *Science of The Total Environment*, *695*, 133805. https://doi.org/10.1016/j.scitotenv.2019.133805

Goldberg, D. L., Lu, Z., Streets, D. G., de Foy, B., Griffin, D., McLinden, C. A., et al. (2019). Enhanced capabilities of TROPOMI NO2 : Estimating NOx from North American cities and power plants. *Environmental Science & Technology*, *53*, 12594–12601. https://doi.org/10.1021/acs.est.9b04488

Goldberg, D. L., Saide, P. E., Lamsal, L. N., de Foy, B., Lu, Z., Woo, J.-H., et al. (2019). A top-down assessment using OMI NO2 suggests an underestimate in the NOx emissions inventory in Seoul, South Korea, during KORUS-AQ. *Atmospheric Chemistry and Physics*, *19*(3), 1801–1818. https://doi.org/10.5194/acp-19-1801-2019

Griffin, D., Zhao, X., McLinden, C. A., Boersma, K. F., Bourassa, A., Dammers, E., et al. (2019). High-resolution mapping of nitrogen dioxide with TROPOMI: First results and validation over the Canadian oil sands. *Geophysical Research Letters*, *46*(2), 1049–1060. https://doi.org/10.1029/2018GL081095

He, H., Hembeck, L., Hosley, K. M., Canty, T. P., Salawitch, R. J., & Dickerson, R. R. (2013). High ozone concentrations on hot days: The role of electric power demand and NOx emissions. *Geophysical Research Letters*, *40*(19), 5291–5294. https://doi.org/10.1002/grl.50967

Herman, J., Abuhassan, N., Kim, J., Kim, J., Dubey, M., Raponi, M., & Tzortziou, M. (2019). Underestimation of column NO2 amounts from the OMI satellite compared to diurnally varying ground-based retrievals from multiple PANDORA spectrometer instruments. *Atmospheric Measurement Techniques*, *12*(10), 5593–5612. https://doi.org/10.5194/amt-12-5593-2019

Heue, K.-P., Richter, A., Bruns, M., Burrows, J. P., Friedeburg, C. V., Platt, U., et al. (2005). Validation of SCIAMACHY tropospheric NO2 columns with AMAXDOAS measurements. *Atmospheric Chemistry and Physics*, *5*, 1039–1051. www.atmos-chem-phys.org/acp/5/1039/SRef-ID:1680-7324/acp/2005-5-1039EuropeanGeosciencesUnion

Ialongo, I., Herman, J. R., Krotkov, N., Lamsal, L. N., Folkert Boersma, K., Hovila, J., & Tamminen, J. (2016). Comparison of OMI NO2 observations and their seasonal and weekly cycles with ground-based measurements in Helsinki. *Atmospheric Measurement Techniques*, *9*(10), 5203–5212. https://doi.org/10.5194/amt-9-5203-2016

Ialongo, I., Virta, H., Eskes, H., Hovila, J., & Douros, J. (2020). Comparison of TROPOMI/Sentinel-5 Precursor NO2 observations with ground-based measurements in Helsinki. *Atmospheric Measurement Techniques*, *13*(1), 205–218. https://doi.org/10.5194/amt-13-205-2020

Jacob, D. J. (2000). Heterogeneous chemistry and tropospheric ozone. *Atmospheric Environment*, *34*(12–14), 2131–2159. https://doi.org/10.1016/S1352-2310(99)00462-8

Judd, L. M., Al-Saadi, J. A., Janz, S. J., Kowalewski, M. G., Pierce, R. B., Szykman, J. J., et al. (2019). Evaluating the impact of spatial resolution on tropospheric NO2 column comparisons within urban areas using high-resolution airborne data. *Atmospheric Measurement Techniques*, *12*, 6091–6111. https://doi.org/10.5194/amt-12-6091-2019

Judd, L. M., Al-Saadi, J. A., Szykman, J. J., Valin, L. C., Janz, S. J., Kowalewski, M. G., et al. (2020). Evaluating Sentinel-5P TROPOMI tropospheric NO2 column densities with airborne and Pandora spectrometers near New York City and Long Island Sound. *Atmospheric Measurement Techniques*, *13*(11), 6113–6140. https://doi.org/10.5194/amt-13-6113-2020

Kleipool, Q. L., Dobber, M. R., de Haan, J. F., & Levelt, P. F. (2008). Earth surface reflectance climatology from 3 years of OMI data. *Journal of Geophysical Research Atmospheres*, *113*(18), 1–22. https://doi.org/10.1029/2008JD010290

Knepp, T., Pippin, M., Crawford, J., Chen, G., Szykman, J., Long, R. W., et al. (2015). Estimating surface NO2 and SO2 mixing ratios from fast-response total column observations and potential application to geostationary missions. *Journal of Atmospheric Chemistry*, *72*(3–4), 261–286. https://doi.org/10.1007/s10874-013-9257-6

Konovalov, I. B., Berezin, E. V., Ciais, P., Broquet, G., Zhuravlev, R. V., & Janssens-Maenhout, G. (2016). Estimation of fossil-fuel CO2 emissions using satellite measurements of "proxy" species. *Atmospheric Chemistry and Physics*, *16*(21), 13509–13540. https://doi.org/10.5194/acp-16-13509-2016

Krotkov, N. A., Lamsal, L. N., Celarier, E. A., Swartz, W. H., Marchenko, S. V., Bucsela, E. J., et al. (2017). The version 3 OMI NO2 standard product. *Atmospheric Measurement Techniques*, *10*(9), 3133–3149. https://doi.org/10.5194/amt-10-3133-2017

Krotkov, N. A., McLinden, C. A., Li, C., Lamsal, L. N., Celarier, E. A., Marchenko, S. V., et al. (2016). Aura OMI observations of regional SO2 and NO2 pollution changes from 2005 to 2015. *Atmospheric Chemistry and Physics*, *16*(7), 4605–4629. https://doi.org/10.5194/acp-16-4605-2016

Lama, S., Houweling, S., Boersma, K. F., Eskes, H., Aben, I., Denier van der Gon, H. A. C., et al. (2020). Quantifying burning efficiency in megacities using the NO2/CO ratio from the Tropospheric Monitoring Instrument (TROPOMI). *Atmospheric Chemistry and Physics*, *20*(17), 10295–10310. https://doi.org/10.5194/acp-20-10295-2020

Lamsal, L. N. (2020). *OMI/Aura nitrogen dioxide standard product with improved surface and cloud treatments*. Retrieved from https://www.atmos-meas-tech-discuss.net/amt-2020-200/

Lamsal, L. N., Martin, R. V., van Donkelaar, A., Steinbacher, M., Celarier, E. A., Bucsela, E., et al. (2008). Ground-level nitrogen dioxide concentrations inferred from the satellite-borne Ozone Monitoring Instrument. *Journal of Geophysical Research*, *113*(16), 1–15. https://doi.org/10.1029/2007JD009235

Larkin, A., Geddes, J. A., Martin, R. V., Xiao, Q., Liu, Y., Marshall, J. D., et al. (2017). Global land use regression model for nitrogen dioxide air pollution. *Environmental Science and Technology*, *51*(12), 6957–6964. https://doi.org/10.1021/acs.est.7b01148

Laughner, J. L., & Cohen, R. C. (2019). Direct observation of changing NOx lifetime in North American cities. *Science*, *366*(6466), 723–727. https://doi.org/10.1126/science.aax6832

Laughner, J. L., Zare, A., & Cohen, R. C. (2016). Effects of daily meteorology on the interpretation of space-based remote sensing of NO2. *Atmospheric Chemistry and Physics*, *16*(23), 15247–15264. https://doi.org/10.5194/acp-16-15247-2016

Laughner, J. L., Zhu, Q., & Cohen, R. C. (2019). Evaluation of version 3.0B of the BEHR OMI NO2 product. *Atmospheric Measurement Techniques*, *12*(1), 129–146. https://doi.org/10.5194/amt-12-129-2019

Levelt, P. F., Joiner, J., Tamminen, J., Veefkind, J. P., Bhartia, P. K., Zweers, D. C. S., et al. (2018). The ozone monitoring instrument: Overview of 14 years in space. *Atmospheric Chemistry and Physics*, *18*(8), 5699–5745. https://doi.org/10.5194/acp-18-5699-2018

Levelt, P. F., Oord, G. H. J. V. D., Dobber, M. R., Dirksen, R. J., Mälkki, A., VISSER, H., et al. (2006). The ozone monitoring instrument. *IEEE Transactions on Geoscience and Remote Sensing*, *44*(5), 1093–1101. https://doi.org/10.1109/TGRS.2006.872333

Liu, M., Lin, J., Boersma, K. F., Pinardi, G., Wang, Y., Chimot, J., et al. (2019). Improved aerosol correction for OMI tropospheric NO2 retrieval over East Asia: constraint from CALIOP aerosol vertical profile. *Atmospheric Measurement Techniques*, *12*(1), 1–21. https://doi.org/10.5194/amt-12-1-2019

Lin, J., Liu, M. Y., Xin, J. Y., Boersma, K. F., Spurr, R., Martin, R. V., & Zhang, Q. (2015). Influence of aerosols and surface reflectance on satellite NO2 retrieval: Seasonal and spatial characteristics and implications for NOx emission constraints. *Atmospheric Chemistry and Physics*, *15*(19), 11217–11241. https://doi.org/10.5194/acp-15-11217-2015

Liu, F., Page, A., Strode, S. A., Yoshida, Y., Choi, S., Zheng, B., et al. (2020). Abrupt declines in tropospheric nitrogen dioxide over China after the outbreak of COVID-19. *Science Advances*, *6*, eabc2992. https://doi.org/10.1126/sciadv.abc2992

Lorente, A., Boersma, K. F., Eskes, H. J., Veefkind, J. P., van Geffen, J. H. G. M., de Zeeuw, M. B., et al. (2019). Quantification of nitrogen oxides emissions from build-up of pollution over Paris with TROPOMI. *Scientific Reports*, *9*(1), 20033. https://doi.org/10.1038/s41598-019-56428-5

Lorente, A., Folkert Boersma, K., Yu, H., Dörner, S., Hilboll, A., Richter, A., et al. (2017). Structural uncertainty in air mass factor calculation for NO2 and HCHO satellite retrievals. *Atmospheric Measurement Techniques*, *10*(3), 759–782. https://doi.org/10.5194/amt-10-759-2017

Lu, Z., Streets, D. G., de Foy, B., Lamsal, L. N., Duncan, B. N., & Xing, J. (2015). Emissions of nitrogen oxides from US urban areas: Estimation from ozone monitoring instrument retrievals for 2005-2014. *Atmospheric Chemistry and Physics*, *15*(18), 10367–10383. https://doi.org/10.5194/acp-15-10367-2015

Ma, J. Z., Beirle, S., Jin, J. L., Shaiganfar, R., Yan, P., & Wagner, T. (2013). Tropospheric NO2 vertical column densities over Beijing: Results of the first three years of ground-based MAX-DOAS measurements (2008-2011) and satellite validation. *Atmospheric Chemistry and Physics*, *13*(3), 1547–1567. https://doi.org/10.5194/acp-13-1547-2013

Martin, R. V., Chance, K., Jacob, D. J., Kurosu, T. P., Spurr, R. J. D., Bucsela, E., et al. (2002). An improved retrieval of tropospheric nitrogen dioxide from GOME. *Journal of Geophysical Research*, *107*(20). https://doi.org/10.1029/2001JD001027

McConnell, R., Berhane, K., Gilliland, F., London, S. J., Islam, T., Gauderman, W. J., et al. (2002). Asthma in exercising children exposed to ozone: a cohort study. *Lancet (London, England)*, *359*(9304), 386–391. https://doi.org/10.1016/S0140-6736(02)07597-9

McDonald, B. C., Dallmann, T. R., Martin, E. W., & Harley, R. A. (2012). Long-term trends in nitrogen oxide emissions from motor vehicles at national, state, and air basin scales. *Journal of Geophysical Research*, *117*(D21). https://doi.org/10.1029/2012JD018304

McLinden, C. A., Fioletov, V. E., Krotkov, N. A., Li, C., Boersma, K. F., & Adams, C. (2016). A decade of change in NO2 and SO2 over the Canadian oil sands as seen from space. *Environmental Science and Technology*, *50*(1), 331–337. https://doi.org/10.1021/acs.est.5b04985

Mijling, B., & Van Der A, R. J. (2012). Using daily satellite observations to estimate emissions of short-lived air pollutants on a mesoscopic scale. *Journal of Geophysical Research*, *117*(17). https://doi.org/10.1029/2012JD017817

Munro, R., Lang, R., Klaes, D., Poli, G., Retscher, C., Lindstrot, R., et al. (2016). The GOME-2 instrument on the Metop series of satellites: instrument design, calibration, and level 1 data processing – An overview. *Atmospheric Measurement Techniques*, *9*(3), 1279–1301. https://doi.org/10.5194/amt-9-1279-2016

Penn, E., & Holloway, T. (2020). Evaluating current satellite capability to observe diurnal change in nitrogen oxides in preparation for geostationary satellite missions. *Environmental Research Letters*, *15*, 034038. https://doi.org/10.1088/1748-9326/ab6b36

Qu, Z., Henze, D. K., Capps, S. L., Wang, Y., Xu, X., Wang, J., & Keller, M. (2017). Monthly top-down NOx emissions for China (2005-2012): A hybrid inversion method and trend analysis. *Journal of Geophysical Research*, *122*(8), 4600–4625. https://doi.org/10.1002/2016JD025852

Rasool, Q. Z., Bash, J. O., & Cohan, D. S. (2019). Mechanistic representation of soil nitrogen emissions in the Community Multiscale Air Quality (CMAQ) model v 5.1. *Geoscientific Model Development*, *12*, 849–878. https://doi.org/10.5194/gmd-12-849-2019

Reuter, M., Buchwitz, M., Schneising, O., Krautwurst, S., O'dell, C. W., Richter, A., et al. (2019). Towards monitoring localized CO2 emissions from space: Co-located regional CO2 and NO2 enhancements observed by the OCO-2 and S5P satellites. *Atmospheric Chemistry and Physics*, *19*, 9371–9383. https://doi.org/10.5194/acp-19-9371-2019

Richter, A., Begoin, M., Hilboll, A., & Burrows, J. P. (2011). An improved NO2 retrieval for the GOME-2 satellite instrument. *Atmospheric Measurement Techniques*, *4*(6), 1147–1159. https://doi.org/10.5194/amt-4-1147-2011

Richter, A., & Burrows, J. P. (2002). Tropospheric NO2 from GOME measurements. *Advances in Space Research*, *29*, 1673–1683. Retrieved from www.eIsevier.com/locatelasr

Romer, P. S., Duffey, K. C., Wooldridge, P. J., Edgerton, E., Baumann, K., Feiner, P. A., et al. (2018). Effects of temperature-dependent NOx emissions on continental ozone production. *Atmospheric Chemistry and Physics*, *18*(4), 2601–2614. https://doi.org/10.5194/acp-18-2601-2018

Russell, A. R., Perring, A. E., Valin, L. C., Bucsela, E. J., Browne, E. C., Wooldridge, P. J., & Cohen, R. C. (2011). A high spatial resolution retrieval of NO2 column densities from OMI: Method and evaluation. *Atmospheric Chemistry and Physics*, *11*(16), 8543–8554. https://doi.org/10.5194/acp-11-8543-2011

Russell, A. R., Valin, L. C., Bucsela, E. J., Wenig, M. O., & Cohen, R. C. (2010). Space-based constraints on spatial and temporal patterns of NOx emissions in California, 2005-2008. *Environmental Science and Technology*, *44*(9), 3608–3615. https://doi.org/10.1021/es903451j

Shah, V., Jacob, D. J., Li, K., Silvern, R. F., Zhai, S., Liu, M., et al. (2020). Effect of changing NOx lifetime on the seasonality and long-term trends of satellite-observed tropospheric NO2 columns over China. *Atmospheric Chemistry and Physics Discussions*, *20*(3), 1483–1495. https://doi.org/10.5194/acp-2019-670

Souri, A. H., Choi, Y., Jeon, W., Li, X., Pan, S., Diao, L., & Westenbarger, D. A. (2016). Constraining NOx emissions using satellite NO2 measurements during 2013 DISCOVER-AQ Texas campaign. *Atmospheric Environment*, *131*(2), 371–381. https://doi.org/10.1016/j.atmosenv.2016.02.020

Stavrakou, T., Müller, J.-F., Bauwens, M., Boersma, K. F., & van Geffen, J. (2020). Satellite evidence for changes in the NO2 weekly cycle over large cities. *Scientific Reports*, *10*(1), 10066. https://doi.org/10.1038/s41598-020-66891-0

Stavrakou, T., Müller, J.-F., Boersma, K. F., De Smedt, I., & van der A, R. J. (2008). Assessing the distribution and growth rates of NOx emission sources by inverting a 10-year record of NO2 satellite columns. *Geophysical Research Letters*, *35*(10). https://doi.org/10.1029/2008GL033521

Timmermans, R., Segers, A., Curier, L., Abida, R., Attié, J.-L., El Amraoui, L., et al. (2019). Impact of synthetic space-borne NO2 observations from the Sentinel-4 and Sentinel-5P missions on tropospheric NO2 analyses. *Atmospheric Chemistry and Physics*, *19*(19), 12811–12833. https://doi.org/10.5194/acp-19-12811-2019

Tzortziou, M. A., Herman, J. R., Cede, A., Loughner, C. P., Abuhassan, N. K., & Naik, S. (2015). Spatial and temporal variability of ozone and nitrogen dioxide over a major urban estuarine ecosystem. *Journal of Atmospheric Chemistry*, *72*(3–4), 287–309. https://doi.org/10.1007/s10874-013-9255-8

Valin, L. C., Russell, A. R., & Cohen, R. C. (2013). Variations of OH radical in an urban plume inferred from NO2 column measurements. *Geophysical Research Letters*, *40*(9), 1856–1860. https://doi.org/10.1002/grl.50267

Valin, L. C., Russell, A. R., & Cohen, R. C. (2014). Chemical feedback effects on the spatial patterns of the NOx weekend effect: A sensitivity analysis. *Atmospheric Chemistry and Physics*, *14*(1), 1–9. https://doi.org/10.5194/acp-14-1-2014

Valin, L. C., Russell, A. R., Hudman, R. C., & Cohen, R. C. (2011). Effects of model resolution on the interpretation of satellite NO2 observations. *Atmospheric Chemistry and Physics*, *11*(22), 11647–11655. https://doi.org/10.5194/acp-11-11647-2011

van Geffen, J., Boersma, K. F., Eskes, H., Sneep, M., ter Linden, M., Zara, M., & Veefkind, J. P. (2020). S5P TROPOMI NO slant column retrieval: method, stability, uncertainties and comparisons with OMI. *Atmospheric Measurement Techniques*, *13*(3), 1315–1335. https://doi.org/10.5194/amt-13-1315-2020

Vandaele, A. C., Hermans, C., Simon, P. C., Carleer, M., Colin, R., Fally, S., et al. (1998). Measurements of the NO2 absorption cross-section from 42 000 cm−1 to 10 000 cm−1 (238–1000 nm) at 220 K and 294 K. *Journal of Quantitative Spectroscopy and Radiative Transfer*, *59*(3–5), 171–184. https://doi.org/10.1016/S0022-4073(97)00168-4

VanDerA, R. J., Eskes, H. J., Boersma, K. F., van Noije, T. P. C., Van Roozendael, M., De Smedt, I., et al. (2008). Trends, seasonal variability and dominant NOx source derived from a ten year record of NO2 measured from space. *Journal of Geophysical Research Atmospheres*, *113*(4), 1–12. https://doi.org/10.1029/2007JD009021

VanGeffen, J. H. G. M., Eskes, H. J., Boersma, K. F., Maasakkers, J. D., & Veefkind, J. P. (2019). TROPOMI ATBD of the total and tropospheric NO2 data products. Retrieved from http://www.tropomi.eu/sites/default/files/files/publicS5P-KNMI-L2-0005-RP-ATBD_NO2_data_products-20190206_v140.pdf

Veefkind, J. P., Aben, I., McMullan, K., Förster, H., de Vries, J., Otter, G., et al. (2012). TROPOMI on the ESA Sentinel-5 Precursor: A GMES mission for global observations of the atmospheric composition for climate, air quality and ozone layer applications. *Remote Sensing of Environment*, *120*(2012), 70–83. https://doi.org/10.1016/j.rse.2011.09.027

Verhoelst, T., Compernolle, S., Pinardi, G., Lambert, J.-C., Eskes, H., Eichmann, K.-U., et al. (2020). *Ground-based validation of the Copernicus Sentinel-5p TROPOMI NO2 measurements with the NDACC ZSL-DOAS, MAX-DOAS and Pandonia global networks* (pp. 1–40). Atmospheric Measurement Techniques Discussions. https://doi.org/10.5194/amt-2020-119

Wang, C., Wang, T., Wang, P., & Rakitin, V. (2020). Comparison and validation of TROPOMI and OMI NO2 observations over China. *Atmosphere*, *11*(6), 636. https://doi.org/10.3390/atmos11060636

Zhao, X., Griffin, D., Fioletov, V., McLinden, C. A., Cede, A., Tiefengraber, M., et al. (2020). Assessment of the quality of TROPOMI high-spatial-resolution NO2 data products in the greater Toronto area. *Atmospheric Measurement Techniques*, *13*(4), 2131–2159. https://doi.org/10.5194/amt-13-2131-2020

Zoogman, P., Liu, X., Suleiman, R. M., Pennington, W. F., Flittner, D. E., Al-Saadi, J. A., et al. (2017). Tropospheric emissions: Monitoring of pollution (TEMPO). *Journal of Quantitative Spectroscopy and Radiative Transfer*, *186*(2017), 17–39. https://doi.org/10.1016/j.jqsrt.2016.05.008